Inorganic Chemistry

ARTICLE

pubs.acs.org/IC

Metal Binding to Ligand-Containing Peptide Nucleic Acids

Zhijie Ma,[†] Frank Olechnowicz,[†] Yury A. Skorik,[‡] and Catalina Achim*[,†]

[†]Department of Chemistry, Carnegie Mellon University, 4400 Fifth Avenue, Pittsburgh, Pennsylvania 15213, United States

[‡]Department of Pharmaceutical Engineering, St. Petersburg State Chemical Pharmaceutical Academy, 14 Prof. Popov Street, St. Petersburg, 197376 Russian Federation

Supporting Information

ABSTRACT:

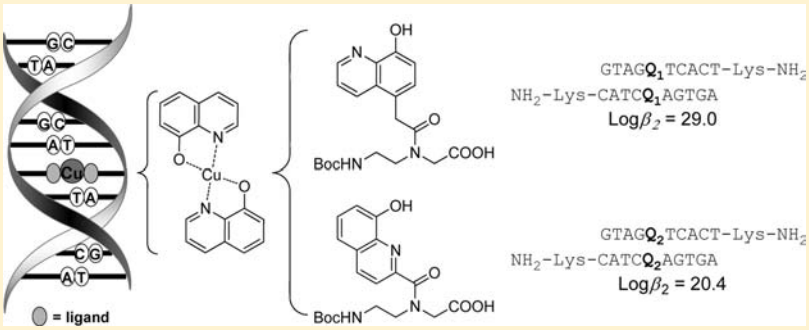

The substitution of nucleobases in nucleic acid duplexes with ligands that have high affinity for transition metal ions creates metal-binding sites at specific locations within the duplexes. Several studies on the incorporation of metal ions into DNA and peptide nucleic acid (PNA) duplexes have suggested that the stability constant of the metal complex formed within the duplexes is a primary determinant of the thermal stability of the duplexes. To understand this relationship, we have synthesized two PNA monomers that carry the same ligand, namely 8-hydroxyquinoline, but have this ligand attached differently to the PNA backbone. The PNA monomers have been incorporated into PNA duplexes. UV and CD spectroscopy and calorimetric studies of the 8-hydroxyquinoline−PNA duplexes showed that the effect of the stability of the metal complex on the PNA duplexes was significantly modulated by the steric relationship between the complex and the duplex. This information is useful for the construction of hybrid inorganic−nucleic acid nanostructures.

INTRODUCTION

The interaction between nucleic acids and transition metal ions can be used to create molecules that have potential applications in nanotechnology and molecular electronics.[1] A strategy for metal ion incorporation into nucleic acid duplexes first proposed by Tanaka and Shionoya in 1999 involves the replacement of the natural nucleobases by ligands that have a higher affinity for metal ions than the natural nucleobases (Scheme 1).[2] The metal complexes formed with these ligand-modified, nucleic acid duplexes can function as metal-mediated, alternative base pairs. If the ligands are aromatic and the geometry of the metal complex is planar, the complexes can participate in π-stacking interactions with adjacent nucleobase pairs. This strategy allows the incorporation of metal ions at specific positions in a nucleic acid duplex,[1,3,4] as well as the creation of arrays of metal ions within a duplex.[5] In the past decade, numerous ligands have been introduced into DNA, RNA, LNA, PNA, and GNA oligomers, and a variety of metal ions have been incorporated into the ligand-modified duplexes formed by these oligomers.[1,3,4,6]

Work in our lab focuses on the use of PNA as a scaffold for metal ions. PNA is a synthetic analogue of DNA that commonly has a backbone based on *N*-(2-aminoethyl)-glycine (Aeg).[7] PNA exhibits a remarkable affinity for complementary DNA and RNA, because its backbone is neutral. In our previous research, methyl bipyridine, bipyridine (Bipy), and 8-hydroxyquinoline (Q) have been introduced into PNA oligomers that formed PNA duplexes containing Ni^{2+}, Co^{2+}, or Cu^{2+}.[8−10] We determined that the thermal stability of the metal-containing, bipyridine−PNA duplexes correlates with the stability constant of the corresponding metal complexes,[8] which is in agreement with results obtained in studies of metal incorporation into DNA duplexes.[4] For example, DNA duplexes containing 2′-deoxyribosyl-*N*9-[6-(2′pyridyl)-purine)] (Pur^P) or 2′-deoxyribosyl-*N*1-[4-(2′pyridyl)-pyrimidinone)] (Pyr^P) have been stabilized in the presence of Ni^{2+} to approximately the same extent despite the fact that the geometry of the Ni^{2+}−Pur^P complex can match that of the base pair in DNA, while the Ni^{2+}−Pyr^P complex has a geometry dissimilar from that of the base pair (Scheme 2a,b).[11,12] The high stability of the duplex that contains the Ni^{2+}−Pyr^P complex was attributed to the strong coordination bonds and the stacking interactions that occur between the ligands and base pairs and may

Received: January 20, 2011
Published: June 02, 2011

compensate for the steric constraint exerted by the complex on the DNA duplex.[12]

In other metal-containing nucleic acid duplexes, the geometry of the metal complex appeared also to be a determinant of the stability of the metal-containing nucleic acid duplexes. For example, a PNA duplex in which a central AT base pair was replaced by a $[Ni(bipy)_2]^{2+}$ complex had a lower melting temperature (58 °C) than that of the nonmodified duplex (66 °C), and only 14 °C higher than that of the bipyridine-modified PNA duplex (44 °C). The fact that the stability of the bipyridine-modified duplex in the presence of Ni^{2+} (58 °C) is lower than that of the nonmodified PNA duplex (66 °C) may be due to steric effects because, in a bis-bipyridine metal complex, the two bipyridine ligands cannot be coplanar. Titration experiments showed that Ni^{2+} coordinates two bipyridines, although there are no four-coordinate, synthetic $[Ni(bipy)_2]^{2+}$ complexes. It is possible that this unusual coordination is achieved because of steric restraints exerted on the complex by the duplex or that Ni^{2+} reaches six-coordination by recruiting two more donor atoms from adjacent nucleobases, or from molecules of solvent or buffer. In either situation, the two bipyridine ligands cannot be coplanar because all four-coordinate $[Pd(bipy)_2]^{2+}$ complexes are distorted square planar,[13] and in all Ni^{2+} complexes with two separate bipyridines and two monodentate ligands, the two bipyridines are cis to each other and not co-planar. This non co-planar arrangement of the bipyridines in the $[Ni(bipy)_2]^{2+}$ complex can affect the nucleobase pairs adjacent to the complex and reduce the stability of the PNA duplex.

Scheme 1. Cartoon Representation of a Metal-Containing, Ligand-Modified Nucleic Acid Duplex

The relative orientation of the ligand binding sites is also likely to affect the binding of metal ions to the modified nucleic acid. Indeed, the thermal stability of two DNA duplexes, each containing different isomers of salicylaldehyde (Scheme 2c,d) in the same position of the duplex, was affected differently by 1 equiv of Cu^{2+}.[14] Specifically, the thermal stability of the DNA duplex that contained 2′-deoxyribosyl-5-(2-hydroxybenzaldehyde) (Scheme 2c) was about the same regardless of the presence of Cu^{2+} (ΔT_m = +1 °C). In contrast, the duplex that contained 2′-deoxyribosyl-4-(2-hydroxybenzaldehyde) (Scheme 2d) was significantly more stable in the presence of Cu^{2+} than in its absence (ΔT_m = +15 °C).[14] This difference in the thermal stability of duplexes induced by metal coordination to the salicylaldehyde was attributed to the relative orientation of the metal binding sites of the ligands with respect to the DNA backbone, which influences the structural compatibility between the metal complex and the duplex.

Compared to the free ligands, the coordination mode of metal ions with the ligands incorporated into nucleic acid duplexes, as well as the stability constants of the corresponding complexes, can be very different due to the supramolecular chelate effect exerted by the duplex. For example, the stability constants of complexes of pyridine (Py) and Ag^+ are very small, and a $[Ag(Py)_2]^+$ complex does not form in solutions containing micromolar concentrations of Ag^+ and Py.[15] In contrast, at the same concentrations, a $[Ag(Py)_2]^+$ complex formed within DNA duplexes that contained a pair of pyridines in complementary positions.[16] In another example, titrations of PNA duplexes containing one pair of 8-hydroxyquinolines led to the formation of $[CuQ_2]$ complexes at both low and high temperatures. These complexes transformed to [CuQ] complexes in the presence of excess Cu^{2+} only at high temperature, where the double stranded (ds) duplex dissociates in single strands (ss).[10]

Scheme 3. Chemical Structure of (a) 2-(*N*-(*tert*-Butyloxycarbonyl-2-aminoethyl)-2-(8-hydroxyquinolin-5-yl)-acetamido)-acetic Acid, Q_1; (b) 2-(*N*-(2-(*tert*-Butoxycarbonyl-2aminoethyl)-8-hydroxyquinoline-2-carboxamido)-acetic Acid, Q_2; and 2,2′-Isopropylidenedi-8-quinolinol, ipdq

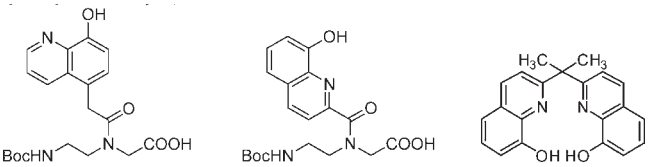

Scheme 2. (a) 2′-Deoxyribosyl-*N*9-[6-(2′pyridyl)-purine)], Pur^P; (b) 2′-Deoxyribosyl-*N*1-[4-(2′pyridyl)-pyrimidinone)], Pyr^P; (c) 2′-Deoxyribosyl-5-(2-hydroxybenzaldehyde); and (d) 2′-Deoxyribosyl-4-(2-hydroxybenzaldehyde)

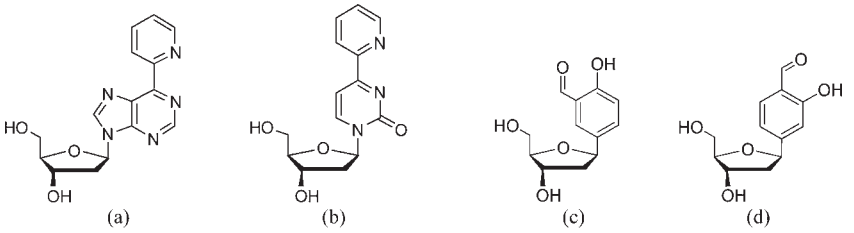

dx.doi.org/10.1021/ic200138b |*Inorg. Chem.* 2011, 50, 6083–6092

The goal of the present research was to systematically examine how steric factors affect the stability of a metal-containing PNA duplex. To achieve this goal, we incorporated into PNA duplexes a pair of 8-hydroxyquinoline ligands, which have been attached to the nucleic acid backbone at different positions and through different linkers (Scheme 3a,b). Our study shows that the interaction between the Q-PNA duplexes and Cu^{2+} depends on (1) the way in which a given ligand is attached to the PNA, and (2) the sequence and/or the structure of the PNA.

RESULTS AND DISCUSSION

Two ligand-containing PNA monomers, $\mathbf{Q_1}$ and $\mathbf{Q_2}$, were synthesized (Scheme 3a,b). Both monomers contain the bidentate ligand 8-hydroxyquinoline, but the attachment of the ligand to the PNA backbone was different in $\mathbf{Q_1}$ and $\mathbf{Q_2}$ (Scheme 3a,b). The monomer $\mathbf{Q_1}$ was synthesized by previously published procedures.[10] The monomer $\mathbf{Q_2}$ was prepared by coupling the acetic acid derivative of 8-hydroxyquinoline **2** with *N*-(2-(*tert*-butoxycarbonyl)-aminoethyl)-glycinate **1** to obtain ester **3**, which was next hydrolyzed (Scheme 4). The synthesis of PNA oligomers, some of which included the $\mathbf{Q_1}$ and $\mathbf{Q_2}$ monomers, was done by solid-phase peptide synthesis using the Boc-protection strategy.[17] For comparison purposes, we have also used published methods to synthesize the four-dentate ligand 2,2′-isopropylidenedi-8-quinolinol (ipdq), which contains two 8-hydroxyquinolines covalently connected to each other through a dimethyl-methylene linker (Scheme 3c).[18,19]

Scheme 4. Synthesis of Monomer Acid Q_2: (a) DCC, DhbtOH; (b) NaOH, MeOH

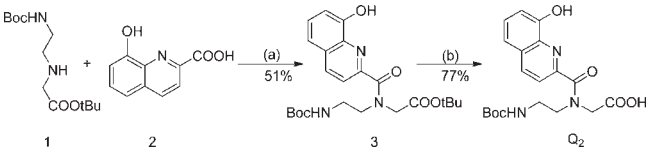

PNA Sequences. The sequences of the nonmodified and Q-PNA oligomers synthesized for this study are listed in Table 1. The 8-hydroxyquinoline monomers $\mathbf{Q_1}$ and $\mathbf{Q_2}$ have been inserted in the middle of a self-complementary PNA oligomer $\mathbf{X_1}$ to create the $\mathbf{Q_1}$- or $\mathbf{Q_2}$-containing oligomers $\mathbf{Q_1}-\mathbf{X_1}$ or $\mathbf{Q_2}-\mathbf{X_1}$, respectively, which in turn can each form a palindromic PNA duplex $\mathbf{Q_1}-\mathbf{X_1}\cdot\mathbf{Q_1}-\mathbf{X_1}$ or $\mathbf{Q_2}-\mathbf{X_1}\cdot\mathbf{Q_2}-\mathbf{X_1}$, respectively. A pair of $\mathbf{Q_1}$, $\mathbf{Q_2}$, or one $\mathbf{Q_1}$ and one $\mathbf{Q_2}$ ligands, has also been introduced in complementary positions in the middle of a PNA duplex based on two complementary PNA oligomers $\mathbf{X_2}$ and $\mathbf{X_3}$ to create the Q-modified, PNA duplexes $\mathbf{Q_1}-\mathbf{X_2}\cdot\mathbf{Q_1}-\mathbf{X_3}$, $\mathbf{Q_2}-\mathbf{X_2}\cdot\mathbf{Q_2}-\mathbf{X_3}$, $\mathbf{Q_1}-\mathbf{X_2}\cdot\mathbf{Q_2}-\mathbf{X_3}$, or $\mathbf{Q_2}-\mathbf{X_2}\cdot\mathbf{Q_1}-\mathbf{X_3}$, respectively. All PNA oligomers had a C-end L-lysine, which exerts a chiral induction effect on the duplexes in solution and improves the solubility of both the ss and ds PNA. PNA hybridization was done in pH 7.0 sodium phosphate or Tris buffers because the PNA duplexes formed under these conditions have been very well characterized.[20−23] Cu^{2+} can coordinate to these buffers, but the stability constants of the complexes formed in the buffers are low when compared to those of the Cu^{2+} complexes with the 8-hydroxyquinoline ligands. Hence, the buffer molecules are not competitive ligands for the Q−PNA, and the stoichiometry and apparent stability constants of the complexes formed between Q−PNA and Cu^{2+} can be determined in these buffers. The absolute stability constants were measured only in Tris buffer because the nature and stability constants of the complexes formed by Cu^{2+} and Tris are known.[15]

Properties of Ligand-Modified PNAs in the Absence of Transition Metal Ions. The UV spectra of the nonmodified PNAs $\mathbf{X_1}\cdot\mathbf{X_1}$ and $\mathbf{X_2}\cdot\mathbf{X_3}$ are dominated by a strong absorption band at 260 nm (red lines in Figure 1). The spectrum of 8-hydroxyquinoline has an absorption band at 239 nm (black lines in Figure 1). The 260 and 239 nm bands correspond to $\pi-\pi^*$ transitions of the nucleobases and of 8-hydroxyquinoline, respectively. These transitions contribute also to the UV spectra of the $\mathbf{Q_1}$-modified PNAs $\mathbf{Q_1}-\mathbf{X_1}\cdot\mathbf{Q_1}-\mathbf{X_1}$ and $\mathbf{Q_1}-\mathbf{X_2}\cdot\mathbf{Q_1}-\mathbf{X_3}$, which showed two absorption bands at 260 and 247 nm (green

Table 1. Melting Temperature [T_m (°C)] and Change in the Melting Temperature [ΔT_m(°C)] for Nonmodified and Q−PNA Duplexes in the Absence or Presence of Metal Ions[a]

duplex	single strand	PNA sequence	no M^{n+} T_m[b]	1 equiv Cu^{2+} T_m[b]	ΔT_m[c]
$\mathbf{X_1}\cdot\mathbf{X_1}$	$\mathbf{X_1}$	H-GGCATGCC-Lys-NH_2	68	68	0
		NH_2-Lys-CCGTACGG-H			
$\mathbf{Q_1}-\mathbf{X_1}\cdot\mathbf{Q_1}-\mathbf{X_1}$	$\mathbf{Q_1}-\mathbf{X_1}$	H-GGCA$\mathbf{Q_1}$TGCC-Lys-NH_2	>75	>75	~8
	$\mathbf{Q_1}-\mathbf{X_1}$	NH_2-Lys-CCGT$\mathbf{Q_1}$ACGG-H			
$\mathbf{Q_2}-\mathbf{X_1}\cdot\mathbf{Q_2}-\mathbf{X_1}$	$\mathbf{Q_2}-\mathbf{X_1}$	H-GGCA$\mathbf{Q_2}$TGCC-Lys-NH_2	>75	>75	~0
	$\mathbf{Q_2}-\mathbf{X_1}$	NH_2-Lys-CCGT$\mathbf{Q_2}$ACGG-H			
$\mathbf{X_2}\cdot\mathbf{X_3}$	$\mathbf{X_2}$	H-GTAGTCACT-Lys-NH_2	63	63	0
	$\mathbf{X_3}$	NH_2-Lys-CATCAGTGA-H			
$\mathbf{Q_1}-\mathbf{X_2}\cdot\mathbf{Q_1}-\mathbf{X_3}$	$\mathbf{Q_1}-\mathbf{X_2}$	H-GTAG$\mathbf{Q_1}$TCACT-Lys-NH_2	46[10]	>79[10]	>33
	$\mathbf{Q_1}-\mathbf{X_3}$	NH_2-Lys-CATC$\mathbf{Q_1}$AGTGA-H			
$\mathbf{Q_2}-\mathbf{X_2}\cdot\mathbf{Q_2}-\mathbf{X_3}$	$\mathbf{Q_2}-\mathbf{X_2}$	H-GTAG$\mathbf{Q_2}$TCACT-Lys-NH_2	38	37	−1
	$\mathbf{Q_2}-\mathbf{X_3}$	NH_2-Lys-CATC$\mathbf{Q_2}$AGTGA-H			
$\mathbf{Q_2}-\mathbf{X_2}\cdot\mathbf{Q_1}-\mathbf{X_3}$	$\mathbf{Q_2}-\mathbf{X_2}$	H-GTAG$\mathbf{Q_2}$TCACT-Lys-NH_2	33	65	32
	$\mathbf{Q_1}-\mathbf{X_3}$	NH_2-Lys-CATC$\mathbf{Q_1}$AGTGA-H			
$\mathbf{Q_1}-\mathbf{X_2}\cdot\mathbf{Q_2}-\mathbf{X_3}$	$\mathbf{Q_1}-\mathbf{X_2}$	H-GTAG$\mathbf{Q_1}$TCACT-Lys-NH_2	44	58	14
	$\mathbf{Q_2}-\mathbf{X_3}$	NH_2-Lys-CATC$\mathbf{Q_2}$AGTGA-H			

[a] The total concentration of ss PNA in each sample was 10 μM. Solutions have been prepared in pH 7.0 10 mM sodium phosphate buffer. [b] The precision for the T_m is ±1 °C. [c] ΔT_m represents the difference between the melting temperature of the duplex formed in the presence and absence of the metal ion.

dx.doi.org/10.1021/ic200138b |*Inorg. Chem.* 2011, 50, 6083–6092

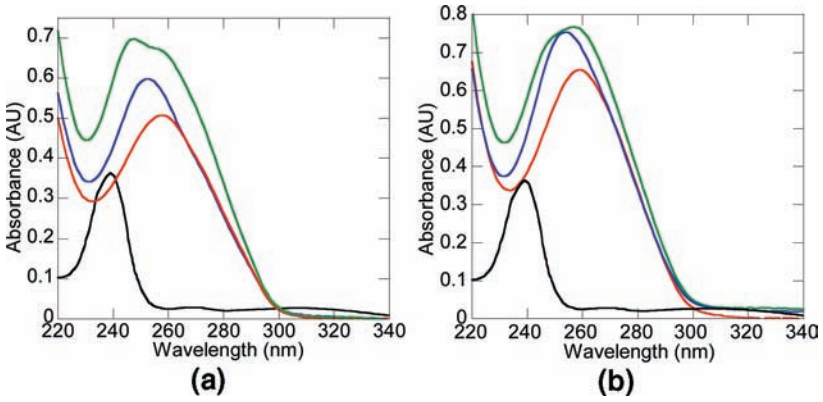

Figure 1. UV absorption spectra of nonmodified and 8-hydroxyquinoline-containing PNA duplexes in pH = 7.0 10 mM sodium phosphate buffer at 25 °C: (a) 5 μM palindromic duplexes 8-base pair duplex $\mathbf{X_1 \cdot X_1}$ (red), 5 μM $\mathbf{Q_2}$−PNA duplex $\mathbf{Q_2}$−$\mathbf{X_1 \cdot Q_2}$−$\mathbf{X_1}$ (blue), 5 μM $\mathbf{Q_1}$−PNA duplex $\mathbf{Q_1}$−$\mathbf{X_1 \cdot Q_1}$−$\mathbf{X_1}$ (green), 10 μM 8-hydroxyquinoline (black); (b) 5 μM nonpalindromic duplexes $\mathbf{X_2 \cdot X_3}$ (red), 5 μM $\mathbf{Q_2}$−PNA duplex $\mathbf{Q_2}$−$\mathbf{X_2 \cdot Q_2}$−$\mathbf{X_3}$ (blue), 5 μM $\mathbf{Q_1}$−PNA duplex $\mathbf{Q_1}$−$\mathbf{X_2 \cdot Q_1}$−$\mathbf{X_3}$ (green), 10 μM 8-hydroxyquinoline (black).

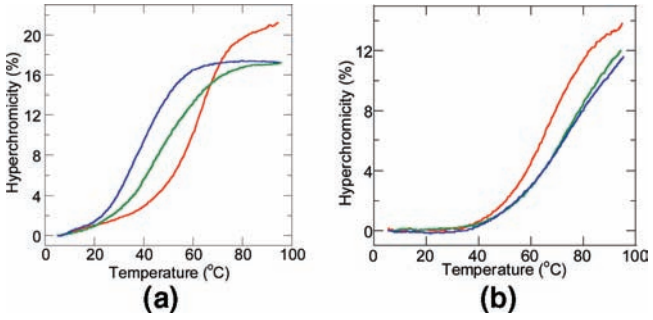

Figure 2. Denaturation profiles measured at 260 nm for 5 μM solutions of (a) $\mathbf{X_2 \cdot X_3}$ (red), $\mathbf{Q_1}$−$\mathbf{X_2 \cdot Q_1}$−$\mathbf{X_3}$ (green), $\mathbf{Q_2}$−$\mathbf{X_2 \cdot Q_2}$−$\mathbf{X_3}$ (blue); (b) $\mathbf{X_1 \cdot X_1}$ (red), $\mathbf{Q_1}$−$\mathbf{X_1 \cdot Q_1}$−$\mathbf{X_1}$ (green), $\mathbf{Q_2}$−$\mathbf{X_1 \cdot Q_2}$−$\mathbf{X_1}$ (blue) in pH = 7.0 10 mM sodium phosphate buffer.

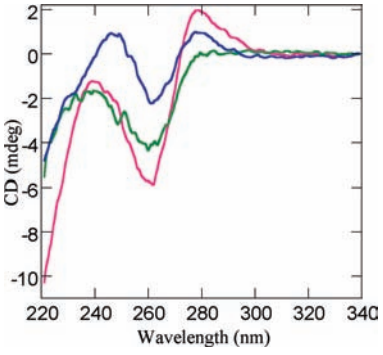

Figure 3. CD spectra of 10 μM $\mathbf{X_1 \cdot X_1}$ (red) and of 10 μM $\mathbf{Q}$−PNA $\mathbf{Q_1}$−$\mathbf{X_1 \cdot Q_1}$−$\mathbf{X_1}$ (green) and 10 μM $\mathbf{Q_2}$−$\mathbf{X_1 \cdot Q_2}$−$\mathbf{X_1}$ (blue) in pH = 7.0 10 mM sodium phosphate buffer, 20 °C.

lines in Figure 1) and of the $\mathbf{Q_2}$-modified PNAs $\mathbf{Q_2}$−$\mathbf{X_1 \cdot Q_2}$−$\mathbf{X_1}$ and $\mathbf{Q_2}$−$\mathbf{X_2 \cdot Q_2}$−$\mathbf{X_3}$, which showed a broad band at 253 nm (blue lines in Figure 1).

The melting curves of the PNA duplexes monitored at 260 nm provided information on the thermal stability of the duplexes (Figure 2 and Table 1). The palindromic, 8-bp PNA duplex $\mathbf{X_1 \cdot X_1}$ was slightly more stable than the 9-bp PNA duplex $\mathbf{X_2 \cdot X_3}$, which we attribute to the higher GC content of the former duplex. A smaller cooperative hyperchromicity change was seen for the melting of the $\mathbf{X_1 \cdot X_1}$ duplex than for the longer $\mathbf{X_2 \cdot X_3}$ duplex (Figure 2). Acetylation of the N-terminus of the PNA oligomer $\mathbf{X_1}$ had a small stabilization effect (ΔT_m = +2 °C) on the palindromic duplex $\mathbf{X_1 \cdot X_1}$ (Figure S1).

Incorporation of a pair of 8-hydroxyquinoline ligands in the middle of the 9-base pair PNA duplex $\mathbf{X_2 \cdot X_3}$ to form $\mathbf{Q_1}$−$\mathbf{X_2 \cdot Q_1}$−$\mathbf{X_3}$, $\mathbf{Q_2}$−$\mathbf{X_2 \cdot Q_2}$−$\mathbf{X_3}$, $\mathbf{Q_1}$−$\mathbf{X_2 \cdot Q_2}$−$\mathbf{X_3}$ or $\mathbf{Q_1}$−$\mathbf{X_2 \cdot Q_2}$−$\mathbf{X_3}$ significantly destabilized the duplex (Figure 2a and Table 1). Incorporation of the same pair of ligands into the 8-bp palindromic duplex $\mathbf{X_1 \cdot X_1}$ to form $\mathbf{Q_1}$−$\mathbf{X_1 \cdot Q_1}$−$\mathbf{X_1}$ or $\mathbf{Q_2}$−$\mathbf{X_1 \cdot Q_2}$−$\mathbf{X_1}$ had an even stronger destabilization effect than it did on $\mathbf{X_2 \cdot X_3}$. Specifically, an increase in absorbance was observed at temperatures above 40 °C for $\mathbf{Q_1}$−$\mathbf{X_1 \cdot Q_1}$−$\mathbf{X_1}$ and $\mathbf{Q_2}$−$\mathbf{X_1 \cdot Q_2}$−$\mathbf{X_1}$, but this increase was not sigmoidal as is typical for cooperative melting (Figure 2b). On the other hand, the CD spectra of annealed solutions of $\mathbf{Q_1}$−$\mathbf{X_1 \cdot Q_1}$−$\mathbf{X_1}$ and $\mathbf{Q_2}$−$\mathbf{X_1 \cdot Q_2}$−$\mathbf{X_1}$ at 20 °C (Figure 3) showed features similar to those reported for left handed PNA duplexes (Figure 3).[21] On the basis of the combination of results of melting temperature and CD spectroscopy experiments, we conclude that at 20 °C the $\mathbf{Q_1}$−$\mathbf{X_1 \cdot Q_1}$−$\mathbf{X_1}$ and $\mathbf{Q_2}$−$\mathbf{X_1 \cdot Q_2}$−$\mathbf{X_1}$ duplexes are formed.

The UV and CD spectra and the melting curves indicate that the effect of ligand modification on PNA duplexes depends both on the duplex sequence, and possibly on the secondary structure of the PNA, as well as on the way in which the ligand is attached to the PNA backbone.

Interaction between Cu^{2+} and Ligand-Modified PNA. UV-monitored, thermal denaturation of the PNA duplexes was also performed in the presence of Cu^{2+}. Cu^{2+} (1 equiv) had no effect on the melting temperature of the nonmodified $\mathbf{X_1 \cdot X_1}$ and $\mathbf{X_2 \cdot X_3}$ duplexes (Table 1). This observation indicates that Cu^{2+} interacts weakly, if at all, with the nonmodified PNA duplexes. Our previous studies have shown that the $\mathbf{Q_1}$−$\mathbf{X_2 \cdot Q_1}$−$\mathbf{X_3}$ PNA duplex was significantly stabilized by Cu^{2+} ions (ΔT_m > 33 °C).[10] The effect of Cu^{2+} on the stability of the $\mathbf{Q_1}$−$\mathbf{X_1 \cdot Q_1}$−$\mathbf{X_1}$ duplex was smaller than its effect on the stability of the $\mathbf{Q_1}$−$\mathbf{X_2 \cdot Q_1}$−$\mathbf{X_3}$ duplex (Figure 4a and Table 1). This difference indicates that the effect of one and the same metal complex on the stability of ligand-modified duplexes depends on the duplex sequence and length.

The stability of the $\mathbf{Q_2}$−$\mathbf{X_1 \cdot Q_2}$−$\mathbf{X_1}$ and $\mathbf{Q_2}$−$\mathbf{X_2 \cdot Q_2}$−$\mathbf{X_3}$ PNA duplexes was affected by Cu^{2+} to a much lesser extent than the stability of the corresponding $\mathbf{Q_1}$−PNA duplexes

dx.doi.org/10.1021/ic200138b |*Inorg. Chem.* 2011, 50, 6083–6092

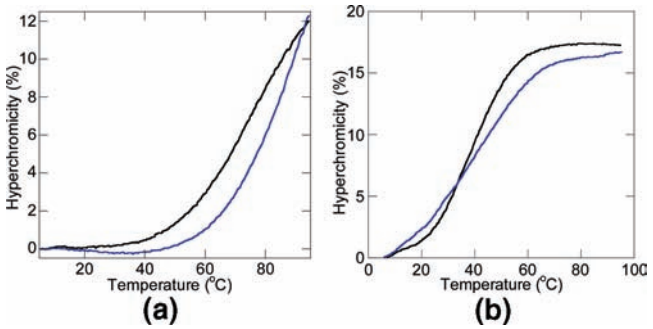

Figure 4. Denaturation profiles measured at 260 nm for (a) 5 μM $\mathbf{Q_1}-\mathbf{X_1}\cdot\mathbf{Q_1}-\mathbf{X_1}$ and (b) 5 μM $\mathbf{Q_2}-\mathbf{X_2}\cdot\mathbf{Q_2}-\mathbf{X_3}$ duplexes in the absence of metal ions (black) and in the presence of 5 μM Cu^{2+} (blue) in pH = 7.0 10 mM sodium phosphate buffer.

$\mathbf{Q_1}-\mathbf{X_1}\cdot\mathbf{Q_1}-\mathbf{X_1}$ and $\mathbf{Q_1}-\mathbf{X_2}\cdot\mathbf{Q_1}-\mathbf{X_3}$ (Figures 4b and S2). Comparison of the melting curves of $\mathbf{Q_2}$−PNA duplexes in the absence and presence of Cu^{2+} showed a negative effect of metal ions on the cooperativity of duplex formation. We further examined the effect of the type of ligand on the duplexes by measuring the melting curves of the two mixed-8-hydroxyquinoline duplexes, $\mathbf{Q_1}-\mathbf{X_2}\cdot\mathbf{Q_2}-\mathbf{X_3}$ or $\mathbf{Q_1}-\mathbf{X_2}\cdot\mathbf{Q_2}-\mathbf{X_3}$, in the presence of Cu^{2+} and observed that as long as at least one of the two 8-hydroxyquinolines is $\mathbf{Q_1}$, the more flexible ligand of the $\mathbf{Q_1}$ and $\mathbf{Q_2}$ pair, Cu^{2+} causes a significant increase in the duplex stability. These results indicate that the way in which the ligands are oriented with respect to the PNA duplex influences significantly the stability of the duplex. The small effect of Cu^{2+} on the $\mathbf{Q_2}$−PNA duplexes and on the $\mathbf{Q_1}-\mathbf{X_1}\cdot\mathbf{Q_1}-\mathbf{X_1}$ duplex could be due to the fact that the formation of an intramolecular $[CuQ_2]$ complex in these duplexes poses a significant steric constraint on the duplex, which compensates the stabilization of the duplex by the metal-based alternative base pair, or that the $[CuQ_2]$ complexes formed with these PNAs are not intraduplex but are inter-duplex.

Titrations of the unmodified $\mathbf{X_1}\cdot\mathbf{X_1}$ PNA duplex with Cu^{2+} caused very small changes in absorption (Figure S3), which suggests that Cu^{2+} interacted very weakly with the $\mathbf{X_1}\cdot\mathbf{X_1}$ PNA duplex. This result is in agreement with the fact that the melting temperature of $\mathbf{X_1}\cdot\mathbf{X_1}$ was not affected by Cu^{2+}. In contrast, the titrations of all of the Q−PNA duplexes with Cu^{2+} led to major changes in the UV−vis spectra of the duplexes, specifically the appearance of a metal-to-ligand charge-transfer band at about 400 nm, which is characteristic for the $[CuQ_2]$ complex (Figures 5, S4, and S5).[10] The formation of $[CuQ_2]$ was supported by the observation of isosbestic points for Cu^{2+}/Q−PNA duplex ratios between 0:1 and 1:1 and of inflection points in the UV−vis titration curves at a Cu^{2+}/Q−PNA duplex ratio of 1:1 (Figure 5c,d). This result is corroborated by EPR spectroscopy. EPR spectra have been recorded for 200 μM solutions of the PNA duplexes $\mathbf{Q_1}-\mathbf{X_1}\cdot\mathbf{Q_1}-\mathbf{X_1}$, $\mathbf{Q_2}-\mathbf{X_1}\cdot\mathbf{Q_2}-\mathbf{X_1}$, or $\mathbf{Q_2}-\mathbf{X_2}\cdot\mathbf{Q_2}-\mathbf{X_3}$ annealed in the presence of 1 equiv of Cu^{2+} (Figure S6), and showed three g values $g_1 \sim g_2 < g_3$, which are very close to those previously measured for $[CuQ_2]$ complexes (Table S2).[24] The concentration of the coordinated Cu^{2+} in solutions of each of the three Q−PNA duplexes determined by double integration of the EPR signal was 191, 202, and 190 μM, respectively, confirming that all Cu^{2+} was within $[CuQ_2]$ complexes formed with the Q−PNA duplexes.

The apparent stability constants of the Cu^{2+} complexes formed with Q−PNA duplexes have been determined by simulations of the UV titrations (Table 2). The constants decreased in the order $\mathbf{Q_1}-\mathbf{X_2}\cdot\mathbf{Q_1}-\mathbf{X_3} > \mathbf{Q_1}-\mathbf{X_1}\cdot\mathbf{Q_1}-\mathbf{X_1} > \mathbf{Q_2}-\mathbf{X_2}\cdot\mathbf{Q_2}-\mathbf{X_3} \approx \mathbf{Q_2}-\mathbf{X_1}\cdot\mathbf{Q_2}-\mathbf{X_1}$, which corroborates the facts that these constants depend on (1) the way in which the ligand is attached to the backbone, with $\mathbf{Q_1}$−PNAs forming more stable complexes than $\mathbf{Q_2}$-PNAs, and (2) the sequence of the PNAs, with $\mathbf{Q}-\mathbf{X_2}\cdot\mathbf{Q}-\mathbf{X_3}$ PNA duplexes forming more stable complexes than the corresponding $\mathbf{Q}-\mathbf{X_1}\cdot\mathbf{Q}-\mathbf{X_1}$ duplexes.

At Cu^{2+}/Q−PNA duplex ratios between 1:1 and 1:2, a new isosbestic point was observed at 258 nm for $\mathbf{Q_2}$−PNA (Figure S4) but not for $\mathbf{Q_1}$−PNA duplexes. This observation indicates that, in the case of $\mathbf{Q_2}$-modified PNA, the $[CuQ_2]$ complexes are converted by excess Cu^{2+} to complexes in which each of the two Q ligands of a duplex coordinates a Cu^{2+} ion. This difference further supports the conclusion that the $[CuQ_2]$ complex formed with $\mathbf{Q_2}$−PNA is less stable than that formed with $\mathbf{Q_1}$−PNA.

We used isothermal titration calorimetry (ITC) to directly measure the thermodynamic parameters for the formation of Cu^{2+} complexes with the free ligand Q, the bitopic ligand ipdq, and Q−PNA in Tris buffer. This buffer was chosen because it is known that Cu^{2+} forms well characterized $Cu(Tris)_4^{2+}$ complexes,[25] whereas Cu^{2+} forms polynuclear complexes in phosphate buffers. Acetonitrile and methanol was added to the solutions of 8-hydroxyquinoline and ipdq to aid in their solubilization. The results of ITC titrations of 8-hydroxyquinoline, ipdq, $\mathbf{Q_1}-\mathbf{X_1}\cdot\mathbf{Q_1}-\mathbf{X_1}$, $\mathbf{Q_2}-\mathbf{X_1}\cdot\mathbf{Q_2}-\mathbf{X_1}$, $\mathbf{Q_1}-\mathbf{X_2}\cdot\mathbf{Q_1}-\mathbf{X_3}$, and $\mathbf{Q_2}-\mathbf{X_2}\cdot\mathbf{Q_2}-\mathbf{X_3}$ with Cu^{2+} are shown in Figures 6 and S8 and the thermodynamic data are compiled in Table 3.[26,27]

The stability constant for the $[CuQ_2]$ complex formed between Cu^{2+} and 8-hydroxyquinoline is in good agreement with the one previously obtained by solubility measurements.[28] The ITC titration of the Q_2 PNA monomer with Cu^{2+} (not shown) showed that it also forms a $[CuQ_2]$ that is only slightly less stable ($\log \beta_2 = 23.4$) than the one formed by the 8-hydroxiquinoline ($\log \beta_2 = 24.6$). The stability constant of the [Cu(ipdq)] complex was 4 orders of magnitude larger than that of the corresponding $[CuQ_2]$ complex formed between Cu^{2+} and 8-hydroxyquinoline, which is due to the chelate effect exerted by the covalent binding of two 8-hydroxyquinoline ligands to each other. We have hypothesized that the chelate effect will also manifest when two 8-hydroxyquinoline ligands are brought into close proximity of each other by the Watson−Crick hybridization of two complementary Q−PNA strands. The ITC results indicate that this hypothesis is correct because the stability constants of the $[CuQ_2]$ complexes formed with $\mathbf{Q_1}-\mathbf{X_1}\cdot\mathbf{Q_1}-\mathbf{X_1}$ or $\mathbf{Q_1}-\mathbf{X_2}\cdot\mathbf{Q_1}-\mathbf{X_3}$ duplexes are 2 and 4 orders of

dx.doi.org/10.1021/ic200138b |*Inorg. Chem.* 2011, 50, 6083–6092

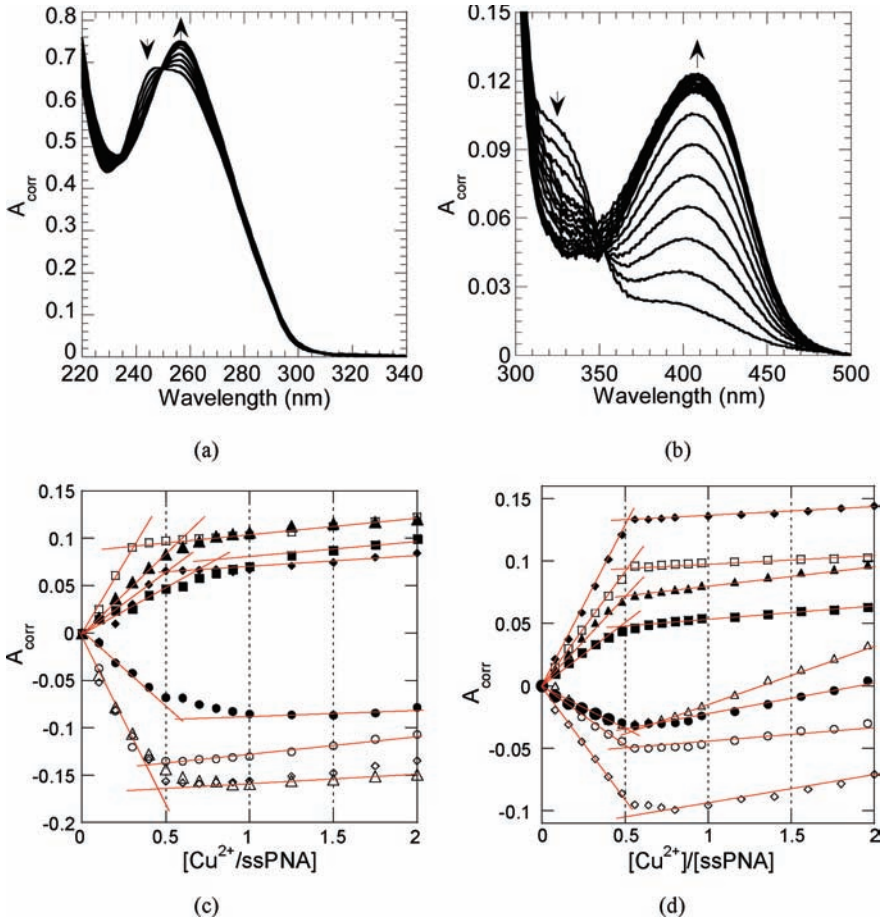

Figure 5. Spectrophotometric titration of a (a) 5 μM and (b) 25 μM $Q_1-X_1\cdot Q_1-X_1$ solution in pH = 7.0 10 mM sodium phosphate buffer with a 0.5 mM or 2.0 mM $Cu(NO_3)_2$ solution in water at 25 °C. (c) Titration curves at 260 nm (□) and 244 nm (○) for $Q_1-X_1\cdot Q_1-X_1$, at 274 nm (■) and 250 nm (●) for $Q_2-X_1\cdot Q_2-X_1$, at 260 nm (◆) and 247 nm (◇) for $Q_1-X_2\cdot Q_1-X_3$, and at 272 nm (▲) and 247 nm (△) for $Q_2-X_2\cdot Q_2-X_3$. (d) Titration curves at 410 nm (□) and 332 nm (○) for $Q_1-X_1\cdot Q_1-X_1$, at 403 nm (■) and 342 nm (●) for $Q_2-X_1\cdot Q_2-X_1$, at 412 nm (◆) and 320 nm (◇) for $Q_1-X_2\cdot Q_1-X_3$, and at 403 nm (▲) and 345 nm (△) for $Q_2-X_2\cdot Q_2-X_3$.

Table 2. Apparent Stability Constants of the $[CuQ_2]$ Complexes with Q−PNA Determined from UV Titrations in pH 7.0 10 mM Phosphate Buffer

Q−PNA duplex	wavelengths range used for calculations	$\log \beta_2' \pm$ SD
$Q_1-X_1\cdot Q_1-X_1$	400−420	9.7 ± 0.2
$Q_1-X_2\cdot Q_1-X_3$	400−420	10.6 ± 0.2
$Q_2-X_2\cdot Q_2-X_3$	400−420	8.74 ± 0.05
$Q_2-X_1\cdot Q_2-X_1$	400−420	8.79 ± 0.09

magnitude larger, respectively, than the stability constant for the corresponding complex of Cu^{2+} and 8-hydroxyquinoline. The enthalpy changes ΔH for the formation of $[CuQ_2]$ complexes are similar to those for the complexes with 8-hydroxyquinoline, ipdq, or Q_1−PNA. However, a much larger positive entropy change was observed for the formation of Cu^{2+} complexes with ipdq or Q_1−PNA than for the complex formed with 8-hydroxyquinoline, as expected in the case of a chelate effect.

The $[CuQ_2]$ complex formed within the $Q_1-X_2\cdot Q_1-X_3$ duplex had a much higher stability constant than the corresponding complex of $Q_2-X_2\cdot Q_2-X_3$. The features observed in ITC titrations of $Q_2-X_1\cdot Q_2-X_1$ with Cu^{2+} at PNA concentrations similar to the ones used in the titrations of $Q_1-X_1\cdot X_1$ and $Q_1-X_2\cdot X_3$ were so weak that we could not determine the equilibrium constant and enthalpy change for Cu^{2+} binding to this duplex (Figure S9). The relative order of the apparent stability constants ($\log \beta_2$) of the $[CuQ_2]$ complexes formed with the $Q_1-X_2\cdot Q_1-X_3$, $Q_1-X_1\cdot Q_1-X_1$, and $Q_2-X_2\cdot Q_2-X_3$ duplexes measured by ITC in Tris buffer and by UV titration in phosphate buffer is the same. The fact that the difference between the $\log \beta_2$ of complexes with $Q_1-X_1\cdot Q_1-X_1$ and $Q_2-X_2\cdot Q_2-X_3$ is smaller when measured by UV titrations than by ITC may be due to differences between the secondary structure of $Q_2-X_2\cdot Q_2-X_3$ in solutions with different pH and buffer molecules and in the nature of the Cu^{2+} complexes existent in these different solutions.

Interestingly, ITC titrations of the $Q_1-X_2\cdot Q_1-X_3$ PNA duplex showed a two-step binding process, with the first and second steps leading to complexes with the $Cu^{2+}/Q_1-X_2\cdot Q_1-X_3$ stoichiometry of 1:2 and 1:1, respectively (Figure 6d). One possible explanation for this behavior is that the first step involves the coordination of Cu^{2+} to two Q ligands from different duplexes to form interduplex $[CuQ_2]$ complexes that bridge two $Q_1-X_2\cdot Q_1-X_3$ PNA duplexes into dimers of duplexes, followed by the entropically driven reorganization of the dimers of duplexes into $Q_1-X_2\cdot Q_1-X_3$ PNA duplexes that contain an

dx.doi.org/10.1021/ic200138b |*Inorg. Chem.* 2011, 50, 6083–6092

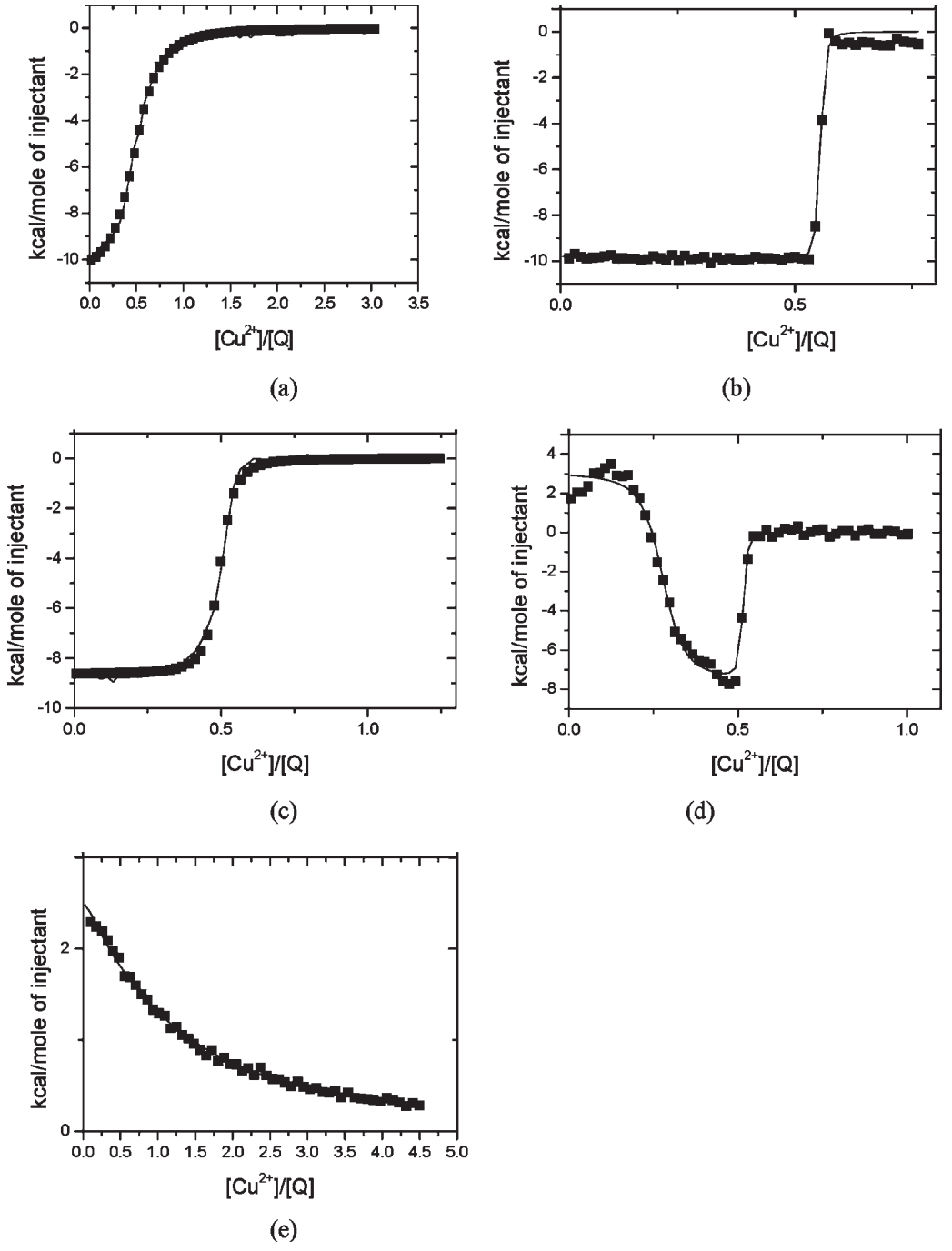

Figure 6. ITC titrations at 25 °C: (a) 0.03 mM 8-hydroxyquinoline with 0.44 mM $Cu(NO_3)_2$ in pH 8.1 3:1 100 mM Tris buffer/acetonitrile, (b) 0.2 mM ipdq with 1.47 mM $Cu(NO_3)_2$ in 1:1 pH 8.1 100 mM Tris buffer/methanol, (c) 0.03 mM $\mathbf{Q_1}-\mathbf{X_1}\cdot\mathbf{Q_1}-\mathbf{X_1}$ with 0.36 mM $Cu(NO_3)_2$ in pH 8.1 100 mM Tris buffer, (d) 0.06 mM $\mathbf{Q_1}-\mathbf{X_2}\cdot\mathbf{Q_1}-\mathbf{X_3}$ with 0.44 mM $Cu(NO_3)_2$ in pH 8.1 100 mM Tris buffer, and (e) 0.06 mM $\mathbf{Q_2}-\mathbf{X_2}\cdot\mathbf{Q_2}-\mathbf{X_3}$ with 1.30 mM $Cu(NO_3)_2$ in pH = 8.1 100 mM Tris buffer.

intramolecular $[CuQ_2]$ complex. A detailed thermodynamic and kinetic study of these phenomena is under way in our lab.

PNA duplexes that have an aminoethyl glycine-based backbone, which is achiral, show a preferred handedness if a chiral amino acid is introduced into the PNA sequence. The chiral induction effect of the amino acid is transmitted through the GC and AT base pairs,[21] or through metal complexes contained within the PNA duplexes.[9,10] The CD spectra of all of the Q—PNA duplexes reported in this study have features indicative of left-handed structures, namely negative peaks at 220 and 255 nm (Figure 7). The small differences in the intensity of the spectra of duplexes that have the same sequence, but contain $\mathbf{Q_1}$ or $\mathbf{Q_2}$ ligands, as well as in the intensity of the spectra of the $\mathbf{Q_1}-\mathbf{X_1}\cdot\mathbf{Q_1}-\mathbf{X_1}$ and $\mathbf{Q_1}-\mathbf{X_2}\cdot\mathbf{Q_1}-\mathbf{X_3}$ duplexes annealed in the presence of Cu^{2+}, suggest the presence of some structural differences between these duplexes. We note at this juncture that the EPR spectra of the $\mathbf{Q_1}-\mathbf{X_1}\cdot\mathbf{Q_1}-\mathbf{X_1}$ duplexes annealed in the presence of Cu^{2+} showed superhyperfine structure indicative of the coordination to Cu^{2+}

dx.doi.org/10.1021/ic200138b |*Inorg. Chem.* 2011, 50, 6083–6092

Table 3. Stoichiometry and Thermodynamic Parameters for the Formation of $[CuQ_2]$ Complexes with Ligands and Q−PNAs in pH = 8.1 100 mM Tris Buffer[a]

ligand/duplex	N	log K_{ITC}	ΔH_{ITC} (kcal/mol)	log β_2	ΔH (kcal/mol)	ΔS (cal/mol/deg)	ΔG (kcal/mol)
8-HQ	1.98	5.7	−5.6	24.6	−22	40	−34
ipdq	1.95	7.7	−5.4	28.6	−21	60	−39
$Q_1-X_1 \cdot Q_1-X_1$	2.02	6.8	−4.3	26.9	−19	60	−37
$Q_1-X_2 \cdot Q_1-X_3$	1.96	7.9	−3.3	29.0	−17	77	−40
$Q_2-X_2 \cdot Q_2-X_3$	1.95	3.6	2.1	20.4	−7	70	−28

[a] The transformation from apparent to absolute binding constants was done using the thermodynamic model described in the text. Error ranges for N, log K, and ΔH are 10%, 3%, and 20%, respectively.

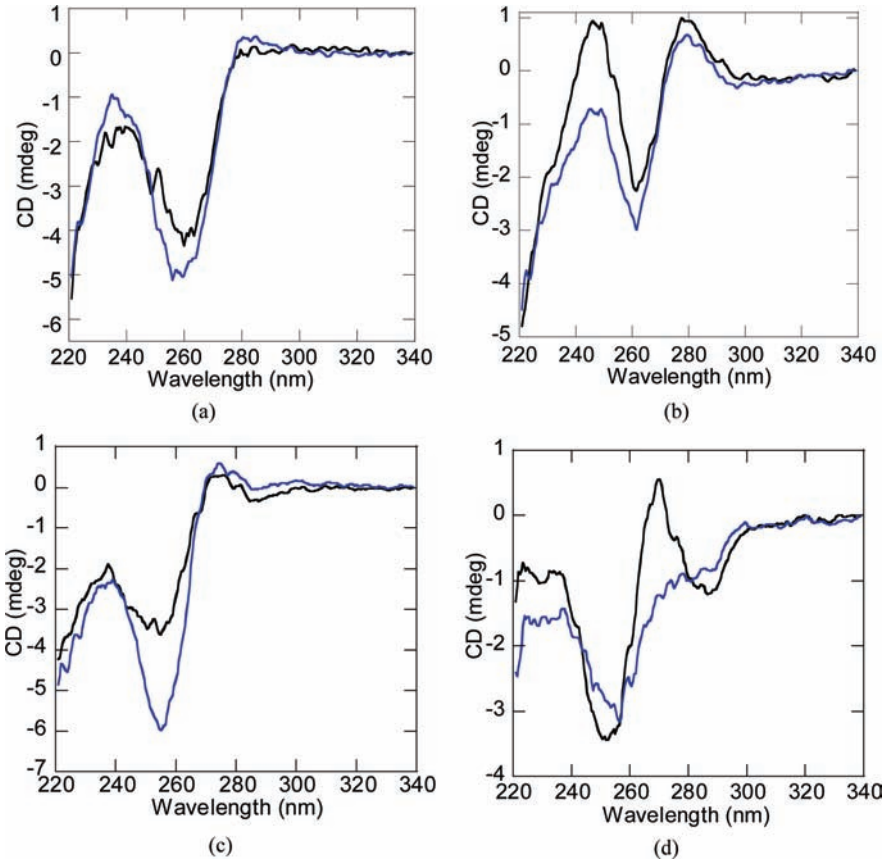

Figure 7. CD spectra of solutions Q−PNA: (a) $Q_1-X_1 \cdot Q_1-X_1$ PNA, (b) $Q_2-X_1 \cdot Q_2-X_1$, (c) $Q_1-X_2 \cdot Q_1-X_3$ PNA, and (d) $Q_2-X_2 \cdot Q_2-X_3$ PNA without (black) and with (blue) 1 equiv Cu^{2+}. All samples are 20 μM ss PNA in pH 7 10 mM sodium phosphate buffer, 20 °C.

of two nitrogen atoms, similar to the structure we have previously observed for $Q_1-X_2 \cdot Q_1-X_3$,[10] while the EPR spectra of Q_2-modified PNAs $Q_2-X_1 \cdot Q_2-X_1-Cu^{2+}$ and $Q_2-X_2 \cdot Q_2-X_3-Cu^{2+}$ showed broad peaks with no superhyperfine features. This difference between the EPR spectra of Q_1−PNA and Q_2−PNA suggests also that there are slight differences between the environment of the $[CuQ_2]$ complexes formed with the Q_2−PNA or Q_1−PNA duplexes. Elucidation of the atomic level details that lead to these differences must await the determination of the structures of these duplexes by NMR spectroscopy or X-ray crystallography.

CONCLUSIONS

The synthesis of nucleic acid duplexes that contain both nucleobase pairs and transition metal complexes is attractive because these hybrid inorganic−nucleic acid structures have properties that are potentially useful for nanotechnology applications. Achieving this potential depends on knowledge of the factors that affect the formation and properties of the hybrid inorganic−nucleic acid structures. Our studies indicate that the propensity of a specific pair of metal ions and ligands to form a complex is maintained when the ligands are introduced into a PNA duplex.

The spectroscopy and thermodynamic studies led to the conclusion that the stability constants of Cu^{2+} complexes with Q−PNA decreased in the order $Q_1-X_2 \cdot Q_1-X_3 > Q_1-X_1 \cdot Q_1-X_1 > Q_2-X_2 \cdot Q_2-X_3 \approx Q_2-X_1 \cdot Q_2-X_1$, which corroborates the fact that these constants depend on (1) the way in which the ligand is attached to the backbone, with Q_1−PNAs forming more stable complexes than Q_2−PNAs, and (2) the sequence of the PNAs, with $Q-X_2 \cdot X_3$ PNA duplexes forming

dx.doi.org/10.1021/ic200138b |Inorg. Chem. 2011, 50, 6083–6092

complexes more stable than the corresponding $\mathbf{Q}-\mathbf{X_1}\cdot\mathbf{X_1}$ duplexes.

Our calorimetric studies showed quantitatively that the Watson−Crick hybridization of two ligand−PNA strands into a duplex can increase the stability constants of the metal complexes formed within the PNA by a few orders of magnitude when compared to the corresponding stability constants for complexes with free ligands. This effect occurs in a manner similar to that in which polytopic ligands form more stable complexes than the corresponding complexes with individual ligands that have the same binding motifs: it is an entropy-driven supramolecular chelate effect. On the other hand, steric constraints limit the supramolecular effect when the relative orientation of the ligands within the PNA duplex does not favor the formation of a metal complex. This modulation effect, which is enthalpic in nature, can be induced both by the sequence/secondary structure of the PNA and by the way in which the ligand is attached to the PNA backbone.

Hence, one can conclude that steric effects, such as those exerted by the change in the linker of the ligand to the PNA backbone, can have substantial effects on the coordination complex formed between the metal and the ligand−PNA duplex and on the stability of the modified PNA duplex. If the relative position of the ligand with respect to the duplex is such that the resulting interstrand metal complex poses high steric demands on the duplex, it is possible that the formation of an interduplex metal complex becomes more favorable than the formation of an alternative metal-based base pair within the duplex or that the stabilization of the duplex by the alternative metal-based base pair is compensated by the destabilization of the duplex by the steric demands. Our study shows that the incorporation of a metal complex with high stability constant into a PNA duplex is not a sufficient condition for the formation of stable hybrid metal−nucleic acid duplexes and that the steric relationship between the complex and the duplex must be considered in the design of metal-containing alternative base pairs.

EXPERIMENTAL SECTION

Materials. All reagents have been obtained from commercially available sources, have been of analytical grade quality, and have been used without further purification. ^{1}H NMR spectra have been recorded on a Bruker Cryospec WM 300. A Finnegan Mattson instrument was used for electrospray mass spectrometry (ES-MS). An Applied Biosystems Voyager biospectrometry workstation with delayed extraction was used for MALDI-TOF mass spectrometry. *tert*-Butyl-*N*-(2-Boc-aminoethyl)-glycinate **1** was prepared according to a published procedure.[20]

Synthesis of *tert*-Butyl-2-(*N*-(2-(*tert*-butoxycarbonyl)ethyl)-8-hydroxyquinoline-2-carboxamido)-acetate (3). 8-Hydroxyquinoline-2-carboxylic acid (100 mg, 0.53 mmol) and 86 mg (0.53 mmol) DhbtOH have been dissolved in 10 mL of DMF. Aeg (146 mg, 0.53 mmol) dissolved in 15 mL of DCM was added to the DMF solution. The resulting solution was cooled to 0 °C, and then 109 mg (0.53 mmol) DCC was added. The solution was stirred at 0 °C for 2 h and then at room temperature for 24 h. The solution was filtered and then diluted with 30 mL of DCM. The resulting solution was washed with a 10% $NaHCO_3$ aqueous solution (25 mL × 3). The organic phase was dried over Na_2SO_4. The DCM was removed under vacuum. The solid obtained after solvent removal was suspended in 20 mL of ethyl acetate. A yellow ethyl acetate solution was obtained after a white precipitate was filtered off. Removal of the ethyl acetate under vacuum led to **1** as orange solid. Yield: 121 mg, 51%. ^{1}H NMR (300 MHz, in *d*-acetone): δ 8.44 (d, J = 8.6 Hz, 1H); 7.94, 7.73 (2d, J = 8.6 Hz, 1H); 7.50−7.60 (m, 1H); 7.48 (dd, J = 1.2, 8.2 Hz, 1H); 7.20 (dd, J = 1.3, 7.6 Hz, 1H); 4.57, 4.24 (2s, 2H, N−CH_2−CO); 3.77 (t, J = 6.4 Hz, 2H, CH_2—N═); 3.30−3.45 (m, 2H, CH_2−NHBoc); 1.29−1.53 (m, 18H, Boc + OtBu). ESI-MS for $(M - H)^-$ (methanol): m/z = 444.1 observed, 444.5 calculated.

Synthesis of 2-(*N*-(2-(*tert*-Butoxycarbonyl)ethyl)-8-hydroxyquinoline-2-carboxamido)-acetic Acid (4). A 1.5 mL portion of a 6 M NaOH solution was added dropwise with constant stirring to a solution of the 8-hydroxyquinoline monomer ester **3** (120.9 mg) in 30 mL 1:2 ethanol−water cooled to 0 °C. The mixture was stirred for 4 h at room temperature. The resulting solution was then filtered, acidified to pH = 4 by addition of 4 M HCl, and extracted with 3 × 30 mL ethyl acetate. The ethyl acetate fractions have been combined, dried over anhydrous Na_2SO_4 and filtered, and the solvent was removed under vacuum to obtain **4** as a yellow solid. Yield: 82 mg, 77%. ^{1}H NMR (300 MHz, in *d*-acetone): δ 8.45 (d, J = 8.6 Hz, 1H); 7.93, 7.73 (2d, J = 8.6 Hz, 1H); 7.50−7.60 (m, 1H); 7.48 (d, J = 7.9 Hz, 1H); 7.19 (t, J = 6.3 Hz, 1H); 4.58, 4.35 (2s, 2H, N−CH_2−CO); 3.70−3.85 (m, 2H, CH_2—N═); 3.30−3.50 (m, 2H, CH_2−NHBoc); 1.31−1.43 (m, 9H, Boc). ES-MS for $(M - H)^-$ (methanol): m/z = 388.1 observed, 388.4 calculated.

PNA Sample Preparation and Storage. PNAs have been dissolved in nanopure water (>18.3 MΩ cm^{-1}) and stored at −18 °C to avoid depurination reactions.

Solid-Phase PNA Synthesis. PNA oligomers have been synthesized using the Boc-protection strategy. PNA monomers have been purchased from Applied Biosystems and ASM Research Chemicals and used without further purification. After cleavage, PNA was precipitated using ethyl ether and was purified by reversed-phase HPLC using a C18 silica column on a Waters 600 controller and pump. Absorbance was measured with a Waters 2996 photodiode array detector. Characterization of the oligomers was performed by MALDI-ToF mass spectrometry on an Applied Biosystems Voyager biospectrometry workstation with delayed extraction and an *R*-cyano-4-hydroxycinnamic acid matrix (10 mg/mL in 1:1 water−acetonitrile, 0.1% TFA). Calculated/found m/z for $(\mathbf{X}_i + H)^+$: $\mathbf{X_1}$ 2314.3/2314.6, $\mathbf{Q_1}-\mathbf{X_1}$ 2600.5/2600.2, $\mathbf{Q_2}-\mathbf{X_1}$ 2586.5/2586.5, $\mathbf{X_2}$ 2579.6/2579.8, $\mathbf{X_3}$ 2588.6/2588.7, $\mathbf{Q_1}-\mathbf{X_2}$ 2865.8/2866.0, $\mathbf{Q_1}-\mathbf{X_3}$ 2874.8/2875.0, $\mathbf{Q_2}-\mathbf{X_2}$ 2851.8/2850.6, $\mathbf{Q_2}-\mathbf{X_3}$ 2860.8/2860.8, $\mathbf{X_4}$ 2356.3/2356.6, $\mathbf{X_5}$ 2628.5/2628.2.

PHYSICAL METHODS

CD Spectroscopy. CD spectra have been measured for 20 μM total PNA concentration in pH 7.0 10 mM sodium phosphate buffer solutions. In the case where complementary PNA strands have been used, solutions have been equimolar in the two strands. CD measurements have been conducted on a JASCO J-715 spectropolarimeter equipped with a thermoelectrically controlled, single-cell holder. CD spectra have been collected using bandwidth 1 nm, response time 1 s, speed 50 nm/min, sensitivity 20 mdeg, and scan accumulation 20.

UV−Vis Spectroscopy. UV−vis experiments have been performed on a Varian Cary 3 spectrophotometer with programmable temperature block, in 10 mm quartz cells. PNA stock solutions have been prepared with nanopure water and have been stored at −18 °C. The concentration of PNA oligomers was determined by UV absorption at 95 °C using the sum of the extinction coefficients of the constituent nucleosides ε_{260} taken from the literature. The extinction coefficient for 8-hydroxyquinoline, ε_{260} = 2570 M^{-1} cm^{-1} (pH = 7.0), was determined from the slope of the calibration curve A_{260} versus concentration. PNA solutions for melting curves and titrations had concentrations in the micromolar range (5−25) and have been prepared in pH 7.0 10 mM phosphate buffer. UV−vis titrations have been carried out by addition of standard 0.5−2 mM $Cu(NO_3)_2$ solutions in water to PNA solutions. The absorbance A after each addition was corrected for dilution and for

dx.doi.org/10.1021/ic200138b |*Inorg. Chem.* 2011, 50, 6083–6092

the contribution of $Cu(NO_3)_2$ and PNA. The PNA solutions for UV−vis spectra have been 10 μM in ss PNA in pH 7 10 mM sodium phosphate buffer unless otherwise noted. The apparent stability constants were calculated from spectrophotometric titration curves by nonlinear regression using the HYPERQUAD 2000 program.[29]

UV melting curves have been recorded in the temperature range 5−95 °C for both cooling and heating modes, at the rate of 1 °C/min. Prior to the measurement of the melting profiles, the solutions have been kept at 95 °C for at least 10 min. Melting curves have been measured at 260 nm. T_m is the inflection point of a sigmoidal function used to fit the melting curve. All measurements have been performed at least in triplicate.

EPR Spectroscopy. EPR spectra have been recorded on an X-band (9 GHz) Bruker ESP 300 spectrometer equipped with an Oxford ESR 910 cryostat. The microwave frequency was calibrated with a frequency counter, and the magnetic field with a NMR gaussmeter. The temperature was calibrated using devices from Lake Shore Cryonics. Spectra have been collected under nonsaturating conditions. Samples have been prepared in pH 7.0 10 mM sodium phosphate buffer with 25% glycerol as glassing agent. Samples containing PNA and Cu^{2+} in appropriate molar ratio have been heated at 95 °C for 10 min, slowly cooled to room temperature, and then transferred into EPR tubes, and frozen. EPR spectra have been simulated using the program SpinCount written by Professor Michael P. Hendrich.[30] Spin quantitation was done relative to a 0.499 mM Na_2[Cu(edta)] standard, the copper concentration of which was determined by plasma emission spectroscopy.

ITC. $Cu(NO_3)_2$ was bought from Alfa Aesar and was 99.999%. 8-Hydroxyquinoline and tris(hydroxymethyl)-aminomethane (Tris) have been obtained from Aldrich and were 99% and 99.9+% pure, respectively. Tris buffer solutions have been made by dissolving calculated amounts of solid in nanopure water, and adjusting to the desired pH with HCl. The concentration of $Cu(NO_3)_2$ was corrected by Cu-EDTA ITC experiment.

A MicroCal VP-ITC was used for all ITC experiments. A sample of one of the solutions was placed in the cell (volume 1.46 mL) and the titrant solution (about 281.5 μM) in a syringe with the stirring speed at 300 rpm. Typically, 58 injections of 5 μL each and 210 s apart were made. The integrated peaks of the heat p have been plotted as a function of the molar ratio. With MicroCal Origin, the binding isotherms have been fitted to a one-site-binding or two-site-binding model, giving values of the enthalpy of binding (ΔH_{ITC}) and the binding constant (K_{ITC}). The binding constants were then corrected taking into consideration the [Cu(Tris)$_4$] complex formation (α_{Cu}, β_4) and the protonation of 8-hydroxyquinoline (α_Q, K_{1H}, K_{2H}).[25]

■ ASSOCIATED CONTENT

Supporting Information. Melting curves of $\mathbf{X_1 \cdot X_1}$, $\mathbf{X_4 \cdot X_4}$, $\mathbf{X_2 \cdot X_3}$; melting curves of $\mathbf{Q_2-X_1 \cdot Q_2-X_1}$, $\mathbf{X_4}$, and $\mathbf{X_5}$ in the absence and presence of Cu^{2+}; UV titrations of $\mathbf{X_1 \cdot X_1}$, $\mathbf{Q_2-X_1 \cdot Q_2-X_1}$, $\mathbf{Q_2-X_2 \cdot Q_2-X_3}$, $\mathbf{X_5 \cdot X_5}$, with Cu^{2+}; ITC of $\mathbf{X_2 \cdot X_3}$ with Cu^{2+}; EPR parameters for [CuQ_2] within PNA context. This material is available free of charge via the Internet at http://pubs.acs.org.

■ AUTHOR INFORMATION

Corresponding Author

*E-mail: achim@cmu.edu. Phone: (412) 268-9588. Fax: (412) 268-1061.

■ ACKNOWLEDGMENT

We thank the U.S. National Science Foundation for support of this work (CHE-0347140). The Center for Molecular Analysis at Carnegie Mellon is supported in part by CHE-9808188. ITC instrumentation was purchased with support from NSF MRI award 0821296. We thank Prof. Mike Hendrich for use of the EPR instruments.

■ REFERENCES

(1) He, W.; Franzini, R. M.; Achim, C. *Prog. Inorg. Chem.* **2007**, *55*, 545–611.
(2) Tanaka, K.; Shionoya, M. *J. Org. Chem.* **1999**, *64*, 5002–5003.
(3) Tanaka, K.; Shionoya, M. *Coord. Chem. Rev.* **2007**, *251*, 2732–2742.
(4) Clever, G. H.; Kaul, C.; Carell, T. *Angew. Chem., Int. Ed.* **2007**, *46*, 6226–6236.
(5) Tanaka, K.; Tengeiji, A.; Kato, T.; Toyama, N.; Shionoya, M. *Science* **2003**, *299*, 1212–1213.
(6) Schlegel, M. K.; Essen, L. O.; Meggers, E. *J. Am. Chem. Soc.* **2008**, *130*, 8158–8159.
(7) Nielsen, P. E.; Egholm, M.; Berg, R. H.; Buchardt, O. *Science* **1991**, *254*, 1497–500.
(8) Franzini, R. M.; Watson, R. M.; Patra, G. K.; Breece, R. M.; Tierney, D. L.; Hendrich, M. P.; Achim, C. *Inorg. Chem.* **2006**, *45*, 9798–9811.
(9) Popescu, D.-L.; Parolin, T. J.; Achim, C. *J. Am. Chem. Soc.* **2003**, *125*, 6354–6355.
(10) Watson, R. M.; Skorik, Y.; Patra, G. K.; Achim, C. *J. Am. Chem. Soc.* **2005**, *127*, 14628–14639.
(11) Switzer, C.; Sinha, S.; Kim, P. H.; Heuberger, B. D. *Angew. Chem., Int. Ed.* **2005**, *44*, 1529–1532.
(12) Switzer, C.; Shin, D. *Chem. Commun.* **2005**, 1342–1344.
(13) Milani, B.; Anzilutti, A.; Vicentini, L.; Santi, A. S.; Zangrando, E.; Geremia, S.; Mestroni, G. *Organometallics* **1997**, *16*, 5064–5075.
(14) Clever, G. H.; Soeltl, Y.; Burks, H.; Spahl, W.; Carell, T. *Chem.—Eur. J.* **2006**, *12*, 8708–8718.
(15) Martell, A. E.; Smith, R. M. *Critical Stability Constants*; Plenum Press: New York, 1976; Vol. 2.
(16) Tanaka, K.; Yamada, Y.; Shionoya, M. *J. Am. Chem. Soc.* **2002**, *124*, 8802–8803.
(17) *Peptide Nucleic Acids: Protocols and Applications*, 2nd ed.; Nielsen, P. E., Ed.; Horizon Bioscience: Wymondham, UK, 2004.
(18) Yamamoto, Y.; Miura, A.; Kawamata, A.; Miura, M.; Takei, S. *Bull. Chem. Soc. Jpn.* **1978**, *51*, 3489–95.
(19) Deraeve, C.; Boldron, C.; Maraval, A.; Mazarguil, H.; Gornitzka, H.; Vendier, L.; Pitie, M.; Meunier, B. *Chem.—Eur. J.* **2008**, *14*, 682–696.
(20) Dueholm, K. L.; Egholm, M.; Behrens, C.; Christensen, L.; Hansen, H. F.; Vulpius, T.; Petersen, K. H.; Berg, R. H.; Nielsen, P. E.; Buchardt, O. *J. Org. Chem.* **1994**, *59*, 5767–73.
(21) Wittung, P.; Eriksson, M.; Lyng, R.; Nielsen, P. E.; Norden, B. *J. Am. Chem. Soc.* **1995**, *117*, 10167–73.
(22) Lagriffoule, P.; Wittung, P.; Eriksson, M.; Jensen, K. K.; Norden, B.; Buchardt, O.; Nielsen, P. E. *Chem.—Eur. J.* **1997**, *3*, 912–919.
(23) Ratilainen, T.; Holmen, A.; Tuite, E.; Haaima, G.; Christensen, L.; Nielsen, P. E.; Norden, B. *Biochemistry* **1998**, *37*, 12331–12342.
(24) Walker, F. A.; Sigel, H.; McCormick, D. B. *Inorg. Chem.* **1972**, *11*, 2756–63.
(25) Zhang, Y.; Akilesh, S.; Wilcox, D. E. *Inorg. Chem.* **2000**, *39*, 3057–3064.
(26) Cu^{2+} interacts very weakly with the nucleobases, and consequently, an ITC titration of the 9-bp $X_2 \cdot X_3$ PNA duplex showed only mixing heat (Figure S7).
(27) The titration of PNA duplexes identical to $\mathbf{Q_2-X_1 \cdot Q_2-X_1}$ except for the N-terminus, which was acetylated, was very similar to that of $\mathbf{Q_2-X_1 \cdot Q_2-X_1}$, which indicates that the acetylation of the terminal amine of the PNA oligomers does not affect the coordination of Cu^{2+} to the $\mathbf{Q_2}$−PNA and excludes the possibility that Cu^{2+} would coordinate to the terminal NH_2 group of the PNA in $\mathbf{Q_2-X_1 \cdot Q_2-X_1}$ rather than to the $\mathbf{Q_2}$ ligands of the $\mathbf{Q_2-X_1 \cdot Q_2-X_1}$ duplex (Figure S6).
(28) Fresco, J.; Freiser, H. *Anal. Chem.* **1964**, *36*, 372–375.
(29) Gans, P.; Sabatini, A.; Vacca, A. *Talanta* **1996**, *43*, 1739–1753.
(30) Hendrich, M. P.; Petasis, D.; Arciero, D. M.; Hooper, A. B. *J. Am. Chem. Soc.* **2001**, *123*, 2997–3005.